Creasing the British museum

Topology finding of crease patterns for shell structures

Oval, Robin; Mesnil, Romain; van Mele, Tom; Baverel, Olivier; Block, Philippe

DOI
10.20898/j.iass.2024.004

Publication date
2024

Document Version
Final published version

Published in
Journal of the International Association for Shell and Spatial Structures

Citation (APA)
Oval, R., Mesnil, R., van Mele, T., Baverel, O., & Block, P. (2024). Creasing the British museum: Topology finding of crease patterns for shell structures. *Journal of the International Association for Shell and Spatial Structures*, *65*(1), 44-56. https://doi.org/10.20898/j.iass.2024.004

JOURNAL OF
THE INTERNATIONAL ASSOCIATION
FOR SHELL AND SPATIAL
STRUCTURES

Prof. D. h-C Eng. E. TORROJA, founder

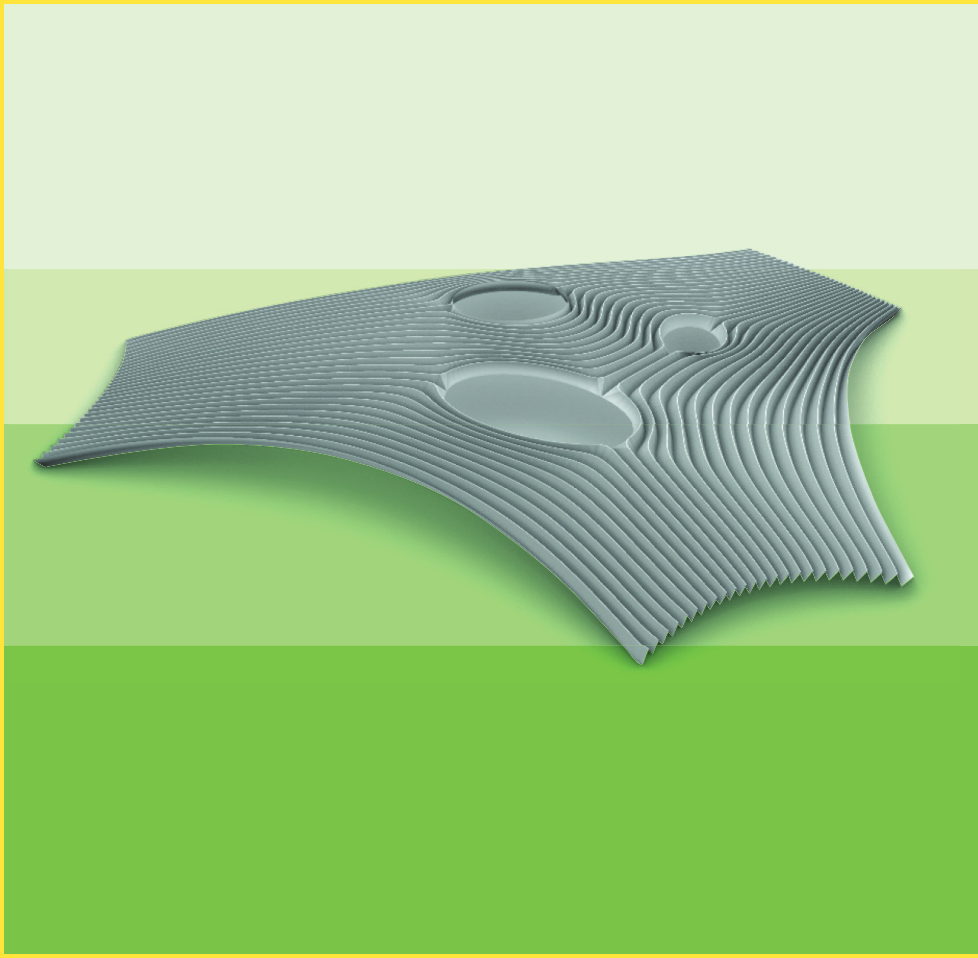

Vol. 65 (2024) No. 1
March n. 219
ISSN: 1028-365X

Journal

VOL. 65 (2024) No. 1
n. 219 March

contents

COVER: *Figures from paper by R. Oval, R. Mesnil, T. Van Mele, O. Baverel and P. Block*

IASS Secretariat: CEDEX-Laboratorio Central de Estructuras y Materiales
Alfonso XII, 3; 28014 Madrid, Spain
Tel: 34 91 3357465; Fax: 34 91 3357422; https://iass-structures.org
journal@iass-structures.org; iass@iass-structures.org
Printed by SODEGRAF ISSN:1028-365X Depósito legal: M. 1444-1960

Vol. 65 (2024) No. 1 March n. 219

CREASING THE BRITISH MUSEUM: TOPOLOGY FINDING OF CREASE PATTERNS FOR SHELL STRUCTURES

Robin OVAL[1], Romain MESNIL[2], Tom VAN MELE[3], Olivier BAVEREL[4] and Philippe BLOCK[5]

[1] Assistant Professor, r.oval@tudelft.nl, TU Delft,
[2] Assistant Professor, romain.mesnil@enpc.fr, Ecole des Ponts ParisTech,
[3] Senior Scientist, van.mele@arch.ethz.ch, ETH Zurich
[4] Professor, olivier.baverel@enpc.fr, Ecole des Ponts ParisTech,
[5] Professor, block@arch.ethz.ch, ETH Zurich

Editor's Note: Manuscript submitted 23 August 2023; revision received 02 November 2023; accepted 17 January 2024. This paper is open for written discussion, which should be submitted to the IASS Secretariat no later than September 2024.

DOI: https://doi.org/10.20898/j.iass.2024.004

ABSTRACT

Several structural systems rely on a specific hierarchy between their constitutive elements, which results in topological constraints on the feasible patterns that can describe them. Folded, corrugated, or creased surface structures require this bipartition, also called two-colouring, between independent wavy and smooth directions. Finding a valid pattern for complex design problems is not straightforward and identifying relevant ones is important as creasing can either strengthen or weaken a structure. This paper presents a way of tackling such a design problem, by focusing on the roof of the Great Courtyard of the British Museum, revisiting this structure with a creased shell to increase its bending stiffness in the key directions. The methodology includes two-colour topology finding of corrugated patterns, parametric structural analysis, and simple structural optimisation through data analysis for topological combination, which opens new research avenues for performance-informed topological exploration.

Keywords: *surface structures, structural design, topological design, creases, folds, corrugations*

1. INTRODUCTION

From leaves in nature to folded paper, introducing curvature and depth through creases and corrugations is an efficient strategy to design stronger and stiffer lightweight structures, as proven by structural engineers and shell builders like Eduardo Torroja, Eladio Dieste, Felix Candela, Heinz Isler, Pier Luigi Nervi, or Nicolas Esquillan. Creased and corrugated shells are part of a larger family of structural systems that rely on sorting their components into two groups, where any pair of elements of the same group are never connected. This partition property is further called *two-colouring*, a name stemming from graph theory map colouring. Two-colouring relates to colouring the elements using only two colours without having adjacent elements of the same colour. Figure 1 illustrates this property for different systems with partitions of panels, beams, and nodes, grouped in red and blue, representing shells, gridshells and other architected structures. This partition also occurs at the scale of the structure of orthotropic architected materials like wood, composite, or textile materials.

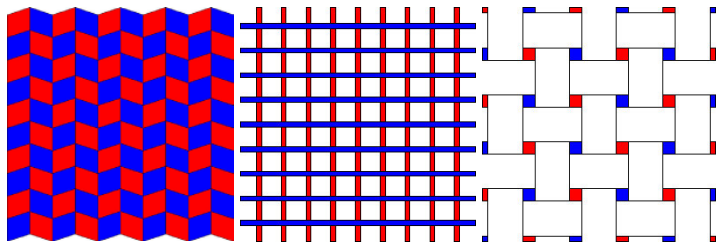

Figure 1: *Two-coloured organisation of elements in patterns based on the partition into two groups, in red and blue*

This property is fulfilled in the case of patterns based on a regular grid, which naturally offers two independent directions of orthogonal elements. However, this property is usually not fulfilled in the case of a general mesh or pattern, particularly for complex design problems of surface structures where a regular grid does not offer an efficient and/or buildable solution.

2. TWO-COLOUR PATTERN DESIGN

Quad-mesh patterns resulting from the integration of cross fields such as curvature fields [1] or stress fields [2] fulfil this two-colour property, by definition. The two groups of elements correspond to the integration of the two orthogonal directions of the cross field. Patterns stemming from such fields are optimal for a specific property, fabrication rationality in the case of curvature fields and structural efficiency in the case of stress fields. Nevertheless, designing two-colour patterns solely through a cross-field is constraining and does not provide the necessary flexibility to explore several design directions and integrate multiple requirements. Oval *et al.* [3] provided a methodology for topology finding of patterns that fulfil this two-colour property for patterns based on quad meshes. The main topological requirements on the pattern are to obtain an even number of strips around each vertex, as well as around each boundary. For efficient computation, a coarse quad mesh is lighter and sufficient, as it discards density but keeps topological singularities, corresponding to nodes with an irregular number of neighbours. Starting from a pattern that can not be two-coloured, two-colouring topology finding yields different patterns that: 1. are two-coloured; 2. are as similar as possible to the input pattern; and 3. provide different design directions. The search approach is based on grammar-based design with the application of rules to add and delete strips of faces in quad meshes, using a graph that represents the connectivity between the strips, and trying to apply a two-colouring algorithm on the graph, to find different combinations that provide this binary alternation. This general approach provides a set of two-colour quad-mesh patterns to investigate. However, their design is not informed by other requirements like mechanical behaviour and structural efficiency, which need to be considered later in the search process for the specific design task. This paper therefore shows an integrated methodology for performance-informed topological exploration of creased shells.

3. CREASING THE BRITISH MUSEUM

We apply two-colour topology finding to creased shells, a structural system that necessitates a two-coloured partition of the pattern to define the creasing directions.

3.1. Mechanics of creased thin plates and shells

Creased, folded, or corrugated shells can efficiently span large areas. The plate in Figure 2 illustrates the differentiated behaviour induced by the introduction of creases, resulting in different geometry and mechanics, interpretable through a virtual separation between membrane and bending behaviour [4]. Along the creases, in red, the structural height is increased, resulting in higher bending stiffness. Across the creases, in blue, the force eccentricity is increased, resulting in a lower membrane stiffness, as in an accordion. Creasing along two transverse directions would yield an egg box pattern that weakens both directions. Therefore, the direction of the folding must be chosen carefully based on the statics system to strengthen the structure and not weaken it. Creasing a structure relying mainly on bi-directional membrane equilibrium like a dome with axial stresses along the meridians and the parallels, weakens it. Creasing a structure relying on bending stiffness can strengthen it, reduce deflection and buckling. Previous research investigated the geometry of the creasing pattern for structural performance and fabrication ease, mainly studying cylindrical surfaces [5-9]. The systematic design of the topology of crease patterns is still unexplored.

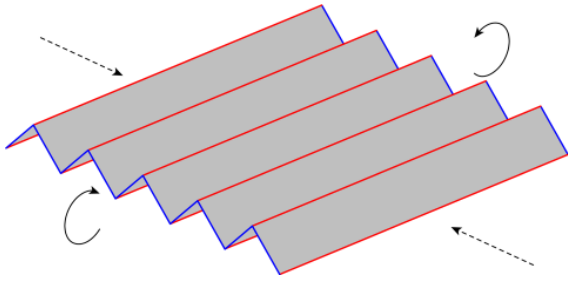

Figure 2: *Crease patterns increase the bending stiffness along the creases (red direction) and decrease the membrane stiffness across them (blue direction)*

3.2. The historical example of the CNIT

Yet, this is crucial, as demonstrated by the CNIT of Nicolas Esquillan built in 1956 at La Défense outside Paris, which spans 218 m, the world record for concrete structures thanks to its double-layer creased design [10]. The CNIT has a triangular footprint with supports at the corners, as illustrated in Figure 3.

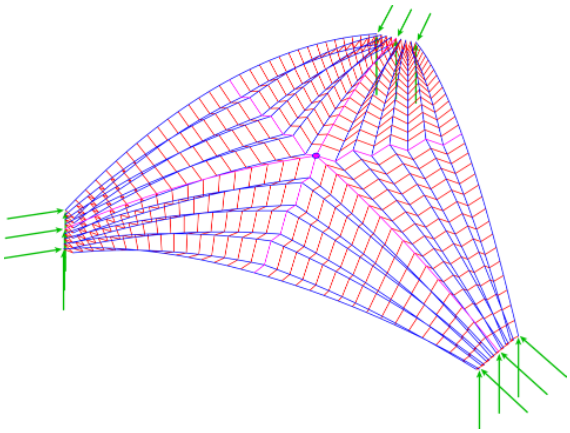

Figure 3: *Principle of the folding pattern of the CNIT. A six-valent singularity in pink provides a two-colour pattern for stiffening the directions that carry the loads along the free edges directly to the supports in green. The stiff smooth directions are shown in blue and the weak creased directions in red*

The folding pattern is designed using a central singularity, in pink, to strengthen the free edges to carry the loads to the supports, in green. The quad mesh serves as parameterisation of the continuous shell to represent its geometry. The stiffened direction is in blue, and the weakened direction is in red. The singularity in the quad mesh that represents and morphs the creased shell has a valency of six. This even number allows the alternation between creased and smooth directions around it. The orientation of the crease directions is essential for structural efficiency.

3.3. The design problem of the British Museum

The 95 m by 74 m roof of the Great Courtyard of the British Museum is vertically supported along its boundary on the existing surrounding buildings, plus horizontally at the four corners of the courtyard, thanks to a boundary truss, avoiding thrust on the walls [11]. The original geometry did not stem from the statics system, as it was analytically defined to smoothly comply with the dictated boundaries [12]. This statics system favours bending behaviour, as opposed to a pure membrane behaviour. Therefore, applying a crease pattern onto the initially smooth surface has the potential to strengthen it by increasing its bending stiffness in the key directions. We revisit this design problem with a concrete shell, finding inspiration from the CNIT.

3.4. Two-colour pattern search

A quad mesh provides a parameterisation of the surface of the shell to morph the creases. Finding a quad mesh with singularities that allows two-colouring is done at the level of a coarse quad mesh where strips of faces represent groups of polyedges, which can be chosen to be creased or smoothed after densification. Skeleton-based decomposition of the initial design surface representing the British Museum does not yield a two-colour pattern [13]. Indeed, the topology of the pattern, shown in Figure 4, with nine coloured strips of quad faces, labelled A to I, representing the coarse quad mesh, has four five-valent singularities that do not allow an even alternation between creased and smooth directions, so that each face is creased along exactly one of its two crossing strips.

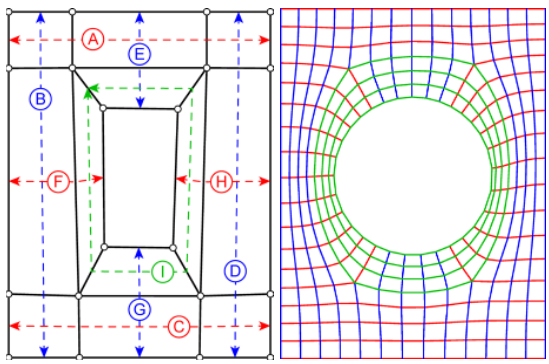

Figure 4: *Coloured meshes from skeleton-based decomposition of the surface with a coarse quad mesh with nine strips. The resulting pattern can not be two-coloured in red and blue only due to the four five-valent singularities that induce a third green colour*

Applying the two-colouring search algorithm to this starting topology yields the nine two-colour topologies in Figure 5. Four of these topologies do not respect the two-fold symmetry of this specific project. Therefore, they are discarded, resulting in a pool of five two-colour topologies. These topologies are the ones most similar to the input while respecting the two-colour requirement by deleting different sets of strips. Nevertheless, further deleting strips yields other two-colour topologies, though less similar to the initial input. The coarse quad meshes have the right set of singularities to produce a crease pattern. More input topological designs could be considered, particularly with pole singularities to attract the creases towards the corners that admit thrust. However, leveraging such topologies is discarded: to avoid having to fabricate high concentrations of creases; to activate bending stiffness through creasing instead of membrane stiffness through external thrust; and to avoid relying on the lateral resistance of the existing building.

The meshes are then densified based on a 1.5 m target length. Closed strips in the coarse quad mesh are divided by an even number to allow a compatible alternation between valleys and mountains. Subsequently, the dense quad meshes are relaxed on the original surface of the British Museum using constrained area-weighted Laplacian surface. The five resulting quad meshes are shown in Figure 6, offering each a parametrisation that provide two different directions for the crease pattern, along either the red curves or the blue ones. For a given direction, the creases result from an alternating offset of the vertices along the corresponding polyedges, following the direction of the local surface normal. Three amplitudes are considered, providing three designs per choice of pattern topology and colour direction: 0.5 m, 1.0 m and 1.5 m. The shells in Figure 7 represent the ten crease patterns, five topologies with two directions each, for the 1.0 m amplitude. The ten designs are labelled X-Y, X representing the pattern topology and Y the crease direction. To summarise, 35 designs are analysed: one smooth, or uncreased, pattern for each of the five parameterisation topologies in Figure 6 and the ten crease patterns in Figure 7 for the three crease amplitudes.

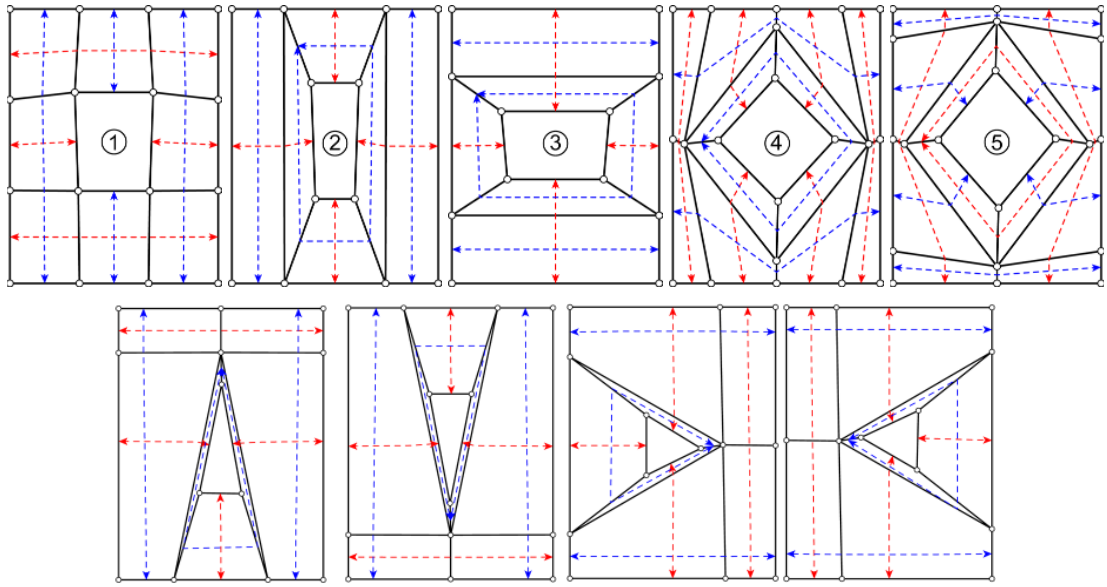

Figure 5: *The five symmetrical (at the top, with labels) and four asymmetrical (at the bottom) two-colour topologies*

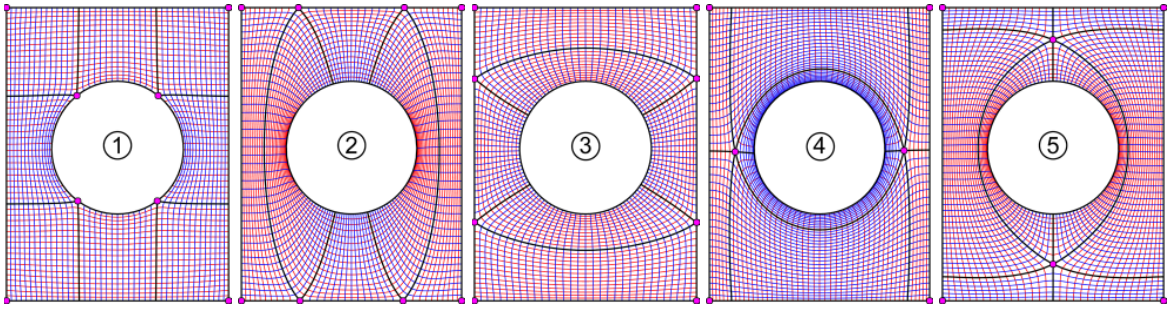

Figure 6: *The five parameterisation quad meshes for the two-colour patterns*

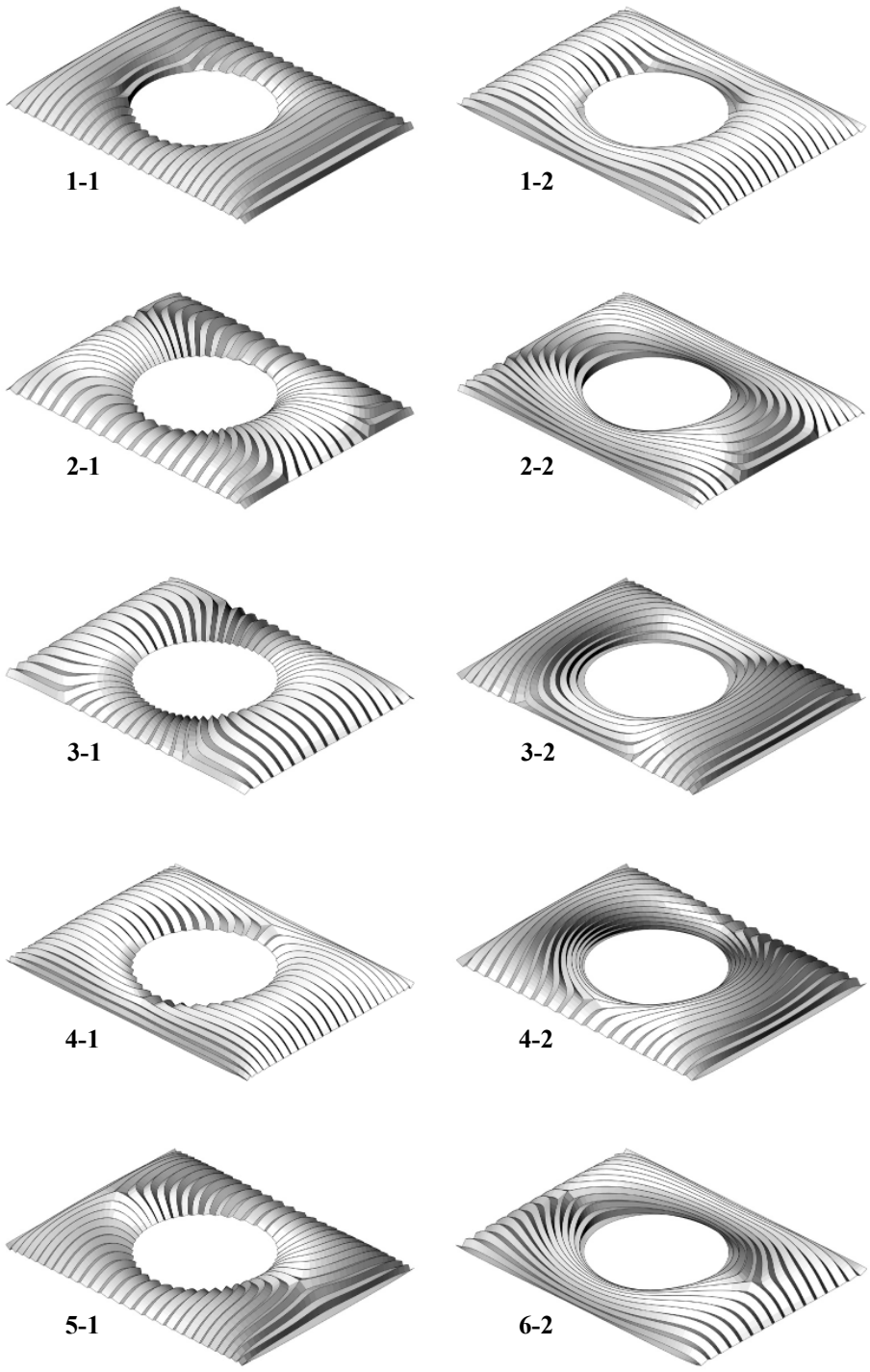

Figure 7: *The ten X-Y creased shells resulting from the five pattern topologies (X) and the two folded directions (Y)*

3.5. Structural performance analysis

A constant mass is set across the designs by adjusting the thickness to avoid bias resulting from a variable self-weight. The constant shell thickness of each design is based on the area of the shell, which depends on the amplitude and the pattern of the creases. A thickness of 20 cm for the medial surface of 6000 m^2 is calibrated to define the constant volume of 1200 m^3, or 3000 t. With a projected area of 5370 m^2, this corresponds to a structural weight of 560 kg/m^2, before any thickness optimisation per design. A C30/37 concrete material is chosen, with a density of 2.5 t/m^3, a characteristic strength f_{ck} of 30 MPa, a Young modulus E_{cm} of 33 GPa and a Poisson coefficient of 0.2. The actual support conditions are considered with full vertical support along the boundary and full horizontal support at the four corners only. A unique load combination is considered, including the self-weight G and a uniform downward projected snow load Q = 0.5 kN/m^2. Geometrical factors for snow distribution resulting from the curved and folded geometry are not considered. A second-order mechanical analysis is performed, using the Finite Element Analysis (FEA) plugin Karamba3D for Grasshopper3D. The quad-mesh pattern is densified and triangulated to produce the FEA shell model. The meshing scheme is applied to refine the quad faces without changing the shape of the shells. A study of the convergence of the strain energy provides the necessary level of refinement, with results shown in Table 1 and Figure 8. The smooth design of topology 1 serves as a test case for all the patterns. A single level of subdivision provides sufficient precision for this analysis without resorting to an unnecessarily large number of faces, as large behaviour influences are investigated, not performance fine tuning.

Table 1: *Results of mesh analysis convergence*

nb subdiv [-]	nb mesh faces [-]	solving time	energy [kN.m]
0	1,932	<1s	262
1	7,728	2-3s	288
2	30,912	10-15s	308
3	123,648	~1.5min	320

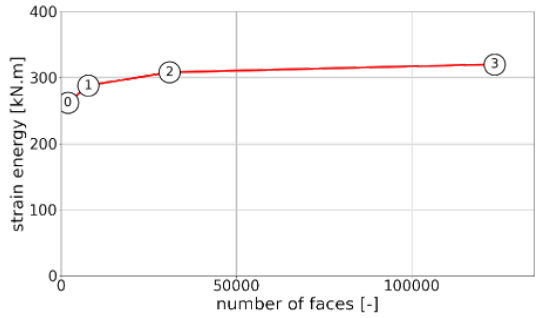

Figure 8: *Mesh analysis convergence per subdivision level*

Four metrics are used to evaluate the structural performance: the maximum displacement, the strain energy, the maximum stress utilisation and the first buckling load factor. Construction aspects and technologies for the creased concrete shell are not considered.

The numerical results from the structural analysis of these 35 designs are detailed in Table 6 in the Appendix. For each topology from 1 to 5, direction 0 provides the smooth design, and directions 1 and 2 provide the two creased designs for amplitudes 0.5 m, 1.0 m, and 1.5 m. The surface area and the thickness all result in the same volume. The parameterisation patterns are refined to obtain the mesh for finite element analysis. The designs are compared based on their strain energy to assess global efficiency: the lower the strain energy, the better the design. Figure 9 compares the strain energy with the amplitude of the creases for each topology–direction combination. The results for a sixth pair of designs are also shown (see Section 3.6). The smooth shells have similar strain energy with an average of 287 kN.m. Their standard deviation equals 5 kN.m, less than 2% of the average, due to the difference in mesh parameterisation only. Creasing transverse directions tends to have an opposite qualitative effect on the structural behaviour, increasing or decreasing the strain energy, highlighted by pairs of solid and dashed curves of the same colour. For instance, folds with an amplitude of 1.5 m in topology 2 decrease the strain energy to 93 kN.m in direction 1 and increase it to 1440 kN.m in direction 2.

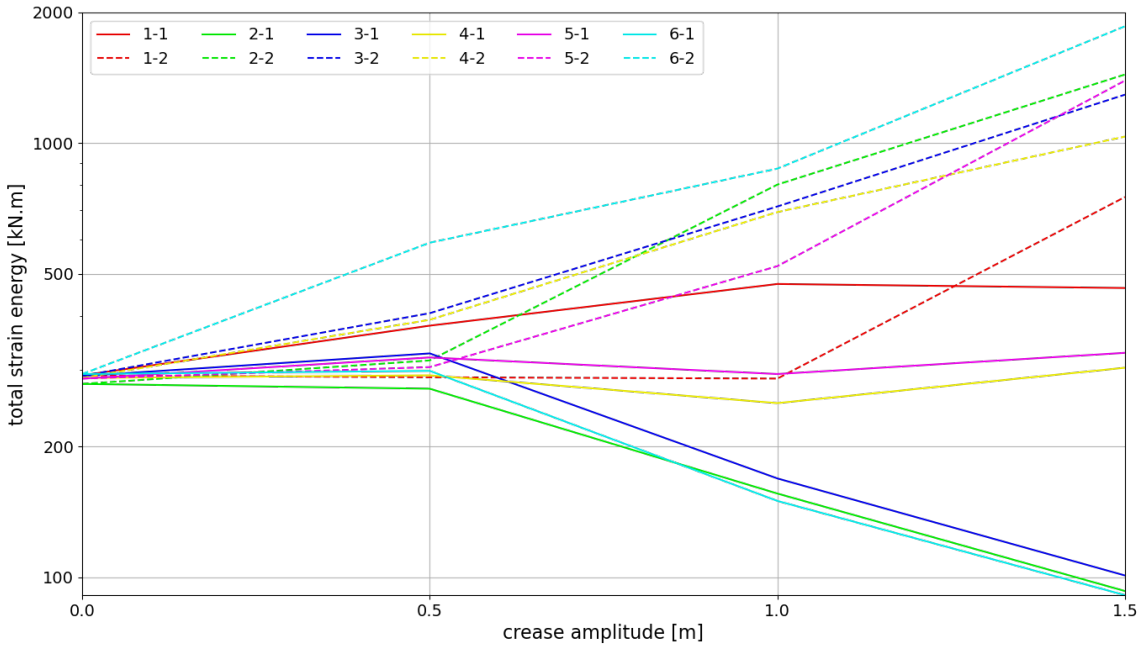

Figure 9: *Influence of the introduction of creases with different topologies, directions, and amplitudes on the total strain energy*

However, the increase or decrease is not monotonic with the amplitude. For instance, creases in topology 3 and direction 1 first increases the strain energy to 328 kN.m for an amplitude of 1.0 m before decreasing to 101 kN.m for an amplitude of 1.5 m, showing a qualitative switch in structural behaviour for creases that are large enough. Notably, most designs increase the strain energy for the high crease amplitude. Nevertheless, two creased designs significantly decrease the strain energy to about one-third of the ones of the smooth designs: topology 2 with direction 1 for an amplitude of 1.5 m resulting in a strain energy of 93 kN.m, and topology 3 with direction 1 for an amplitude of 1.5 m resulting in a strain energy of 101 kN.m. These two designs also perform the best for the other structural metrics. Respectively, they have the lowest maximum deflection, 2.3 and 2.2 cm; the lowest maximum compressive stress utilisation, 0.50 and 0.46, the only ones below 1; and the highest first buckling load factor, 78 and 74. The two most efficient designs, 2-1 and 3-1, are the ones with creases following the shortest spans between the supports on the outer and inner boundaries of the British Museum.

3.6. Pattern combination for structural optimisation

Each topology stems from the deletion of a different sets of strips from the initial design. By connecting the performance of the designs and the deletion rules applied, we aim to further optimise designs by creating hybrid patterns. Intuitively, deletion rules that lead to an improvement in structural performance are combined. Simple data analysis is used to implement this, evaluating the positive or negative contributions to the structural performance of each crease strip across all designs. Specific matrices are built to represent the crease patterns and the performance of each design. Figure 4 shows the A to I labels of the nine strips that form the design space of possible combinations of deletion rules. The matrix in Table 2 represents, for each topology, which strips are present or absent by a 1 or a 0, respectively. The creasing matrix in Table 3 represents, per topology-direction design, which strips are creased by a 1, or by a 0 if not creased or absent, meaning previously deleted. The performance matrix in Table 4 provides the strain energy as a measure of each of the ten crease designs,

averaged across the different values of amplitude. For each strip, the covariance between the creasing matrix (Table 3) and the performance matrix (Table 4) is computed in Table 5. A negative covariance means that folding the strip decreases the strain energy and therefore improves structural behaviour on average, and vice versa. As this covariance per strip is displayed in Figure 10, strips E, F, G, H in green are the only ones that improve the performance on average. Only designs 2-1 and 3-1 feature creases along all these four strips. These designs are the most efficient ones regarding the strain energy metric. Intuitively, these four strips are the only ones that connect the outer and inner boundaries, as previously noted.

Table 2: *Presence matrix of the nine strips for the five topologies: 1 if the strip is present, 0 otherwise*

	1	**2**	**3**	**4**	**5**
A	1	0	1	1	1
B	1	1	0	1	1
C	1	0	1	1	1
D	1	1	0	1	1
E	1	1	1	1	0
F	1	1	1	0	1
G	1	1	1	1	0
H	1	1	1	0	1
I	0	1	1	1	1

The design directions offered by topologies 2 and 3 are therefore the most promising ones for structural performance. These directions are combined to obtain a hybrid topology. Topologies 2 and 3 result from the deletion of strips A and C, and B and D, respectively. Topology 6 in Figure 11 is hence obtained from the deletion of strips A, B, C, and D. With even fewer strips, the topology is also two-colourable. This topology results from the deletion of four strips, as opposed to two for topologies 2 and 3, meaning that it is less similar than the input topological design. The same generation and morphing process is applied to obtain the corresponding pair of creased designs, represented in Figure 12 for the amplitude of 1.0 m. The curves are added to Figure 9 and the complementary numerical results are shown in Table 6. Design 6-1 has creased strips E, F, G, and H, forming creases supported by the two opposite boundaries along the shortest spans. This design offers a strain energy of 91 kN.m, a contribution of axial strain energy of 89%, a displacement of 2.2 cm, a stress utilisation of 0.6, and a first buckling load factor of 39, for the amplitude of 1.5 m. Except for the buckling metric, the other metrics are equal or slightly better than the ones of designs 2-1 and 3-1, for the fold amplitude of 1.5m. The weaker buckling behaviour can be explained by the single curvature of the creases, which are close to the intersections between the smooth surface and a set of radial verticals planes. Indeed, the other creases offer a double curvature that do not have a weaker out-of-plane direction. However, single curvature makes creases easier to build or rationalize into developable strips. The highest contribution from the axial strain energy, as opposed to bending energy, hints at higher compression values overall and supports this analysis. On the contrary, design 6-2 is the worst of all twelve designs regarding strain energy and first buckling load factor. Figures 14 and 15 in the Appendix provide completing curve plots for the axial strain energy and the buckling results for all the shells.

Table 3: *Creasing matrix of the nine strips for the ten crease designs: 1 if the strip is present and folded, 0 otherwise*

	1-1	**1-2**	**2-1**	**2-2**	**3-1**	**3-2**	**4-1**	**4-2**	**5-1**	**5-2**
A	1	0	0	0	0	1	0	1	1	0
B	0	1	0	1	0	0	1	0	0	1
C	1	0	0	0	0	1	0	1	1	0
D	0	1	0	1	0	0	1	0	0	1
E	0	1	1	0	1	0	1	0	0	0
F	1	0	1	0	1	0	0	0	1	0
G	0	1	1	0	1	0	1	0	0	0
H	1	0	1	0	1	0	0	0	1	0
I	0	0	0	1	0	1	0	1	0	1

Table 4: *Performance matrix of the strain energy in kN.m of the ten folded designs averaged across the amplitude values*

	1-1	**1-2**	**2-1**	**2-2**	**3-1**	**3-2**	**4-1**	**4-2**	**5-1**	**5-2**
0	292	292	279	279	291	291	288	288	287	287
0.5	380	289	272	316	328	406	292	392	321	305
1	474	287	156	803	169	715	252	694	294	521
1.5	464	752	93	1440	101	1294	304	1036	329	1394
avrg.	403	405	200	709	222	676	284	602	308	627

Table 5: *Covariance matrix in $kN^2.m^2$ of the energy performance of the creased strips, averaged across all designs*

A	**B**	**C**	**D**	**E**	**F**	**G**	**H**	**I**
21	25	21	25	-66	-64	-66	-64	84

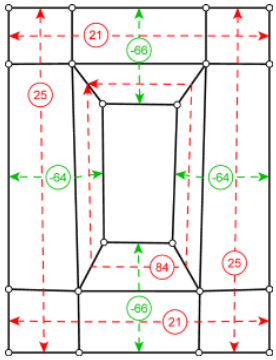

Figure 10: *The covariance in $kN^2.m^2$ of each strip with respect to the strain energy metric when creased*

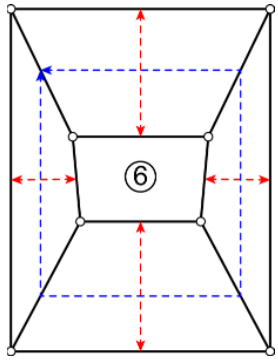

Figure 11: *Sixth symmetrical two-colour topology resulting from the combination of topologies 2 and 3*

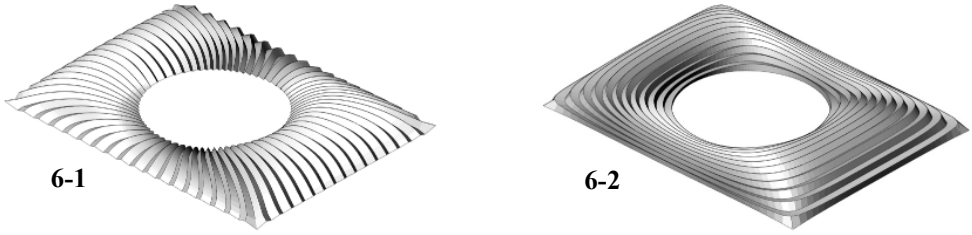

Figure 12: *Two hybrid creased shells resulting from the combination of topologies 2 and 3*

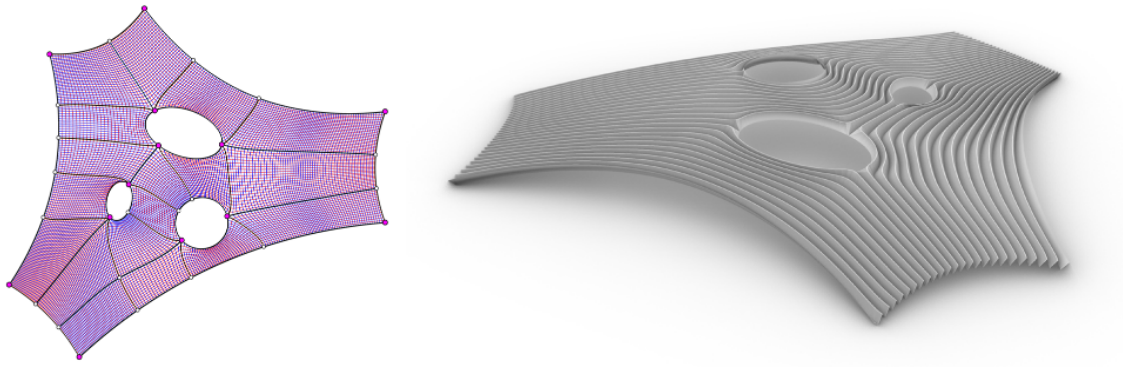

Figure 13: *Pattern topology and render view of a creased shell supported on three sides and with three openings*

4. CONCLUSION

Creases, folds, and corrugations are efficient means to strengthen a thin shell or a plate structure, selectively increasing its structural height and bending stiffness against deflection and buckling. However, finding a relevant pattern that strengthens and does not weaken the structure is not straightforward for complex design problems. This paper presented a means of applying two-colour topology finding to the exploration of crease patterns. The initial set of topological designs was then processed to obtain different crease patterns, their structural performance assessed, and a final pattern obtained as a topological hybrid of the most efficient designs for further structural optimisation. The numerical results showed the structural efficiency of doubly curved creases (for maximum buckling resistance) aligned with the shortest span (for minimum strain energy). In practice, this methodology can be applied to the design of creased shells with more complex boundary conditions (see Figure 13). Furthermore, this study shows the challenge of finding efficient creased shells and the need to allow piecewise smooth geometries in form finding [14]. Beyond creased shells, this methodology serves as an example of designing complex systems where the organisation and hierarchy of the structural pattern is crucial. This work also highlights the potential of data-driven generation of topological hybrids, as a parallel to the approach of parametric breeding in evolutionary algorithms. Future research will investigate a systematic strategy for producing such topological hybrids based on performance data, leveraging graph-based optimisation suitable for grammatical topological design.

REFERENCES

[1] Liu, Y., Pottmann, H., Wallner, J., Yang, Y.L. and Wang, W., 2006. Geometric modeling with conical meshes and developable surfaces. In ACM SIGGRAPH 2006 Papers (pp. 681-689). (DOI: 10.1145/1141911.1141941)

[2] Schiftner, A. and Balzer, J., 2010. Statics-sensitive layout of planar quadrilateral meshes. In Advances in architectural geometry 2010 (pp. 221-236). Springer, Vienna. (DOI: 10.1515/9783990433713-017)

[3] Oval, R., Mesnil, R., Van Mele, T., Block, P. and Baverel, O., 2021. Two-Colour Topology Finding of Quad-Mesh Patterns. *Computer-Aided Design*, *137*, p.103030. (DOI: 10.1016/j.cad.2021.103030)

[4] Calladine, C.R., 1977, September. The static–geometric analogy in the equations of thin shell structures. In Mathematical Proceedings of the Cambridge Philosophical Society (Vol. 82, No. 2, pp. 335-351). Cambridge University Press. (DOI: 10.1017/S0305004100053974)

[5] Norman, A.D., Seffen, K.A. and Guest, S.D., 2009. Morphing of curved corrugated shells. *International Journal of Solids and Structures*, *46*(7-8), pp.1624-1633. (DOI: 10.1016/j.ijsolstr.2008.12.009)

[6] Malek, S. and Williams, C., 2017. The equilibrium of corrugated plates and shells. *Nexus Network Journal*, *19*, pp.619-627. (DOI: 10.1007/s00004-017-0347-7)

[7] Stitic, A. and Weinand, Y., 2015. Timber folded plate structures–topological and structural considerations. *International Journal of Space Structures*, *30*(2), pp.169-177. (DOI: 10.1260/0266-3511.30.2.169)

[8] Mesnil, R., Baverel, O., Douthe, C., Caron, J.F. and Léger, B., 2017. Structural morphology and performance of plated structures with planar quadrilateral facets. *Journal of the International Association for Shell and Spatial Structures*, *58*(1), pp.7-22. (DOI: 10.20898/j.iass.2017.191.845)

[9] Mesnil, R., Douthe, C., Richter, C. and Baverel, O., 2018. Fabrication-aware shape parametrisation for the structural optimisation of shell structures. *Engineering Structures*, *176*, pp.569-584. (DOI: 10.1016/j.engstruct.2018.09.026)

[10] Motro, R. and Maurin, B., 2011, September. Bernard Laffaille, Nicolas Esquillan, Two French Pioneers. In *IASS-IABSE Symposium: Taller, Longer, Lighter*.

[11] Sischka, J., Brown, S., Handel, E. and Zenkner, G., 2001. Die Überdachung des Great Court im British Museum in London. *Stahlbau*, *70*(7), pp.492-502. (DOI: 10.1002/stab.200101690)

[12] Williams, C.J., 2001. The analytic and numerical definition of the geometry of the British Museum Great Court Roof. *Mathematics & design*, *200*, pp.434-440. ISBN: 0-7300-2526-8.

[13] Oval, R., Rippmann, M., Mesnil, R., Van Mele, T., Baverel, O. and Block, P., 2019. Feature-based topology finding of patterns for shell structures. *Automation in Construction*, *103*, pp.185-201. (DOI: 10.1016/j.autcon.2019.02.008)

[14] Hayashi, K., Jikumaru, Y., Ohsaki, M., Kagaya, T. and Yokosuka, Y., 2023. Mean curvature flow for generating discrete surfaces with piecewise constant mean curvatures. Computer Aided Geometric Design, 101, p.102169. (DOI: 10.1016/j.cagd.2023.102169)

APPENDIX

Table 6 provides the numerical results of the performance analysis of the 42 shell designs: six smooth designs plus six creased designs times two folding directions times three amplitudes.

Figures 14 and 15 provide the results regarding the contribution of the axial energy in the total energy and the first buckling load factor, respectively.

The labels of each design describe the topology (between 1 and 6), the creasing direction (1 or 2, or 0 if smooth) and creasing amplitude (0.5 m, 1.0 m, or 1.5 m). The provided shell area and the thickness respect a constant volume. The number of faces is the one of the refined mesh for finite element analysis. The structural performance is evaluated based on the strain energy and completed by the maximum deflection, the maximum stress utilisation, and the first buckling load factor.

Table 6: *Numerical results from the structural analysis of the shell designs. The colour gradient shows the performance per metric relative to the other designs, best in green and worst in red.*

pattern topology	crease direction	crease amplitude [m]	mesh area [m^2]	shell thickness [cm]	shell volume [m^3]	max displacement [cm]	total strain energy [kN.m]	axial strain energy ratio [-]	first buckling load factor [-]	max comp stress [MPa]	max tens stress [MPa]
1	0	0.0	6001	20	1200	4.2	292	0.67	18.3	-73.4	39.3
1	1	0.5	6210	19	1180	6.4	380	0.6	29.8	-75.8	29.2
1	1	1.0	6800	18	1224	9.1	474	0.64	25.7	-56.3	17.4
1	1	1.5	7686	16	1230	11.3	464	0.61	28.3	-36.4	19.1
1	2	0.5	6279	19	1193	3.4	289	0.66	25.7	-60	21.9
1	2	1.0	7047	17	1198	6.8	287	0.52	23.6	-33.2	14.1
1	2	1.5	8149	15	1222	17.5	752	0.47	20.7	-46.9	45.3
2	0	0.0	6000	20	1200	4	279	0.67	18.3	-76.7	39.2
2	1	0.5	6242	19	1186	5.6	272	0.65	47.4	-51.9	17.2
2	1	1.0	6894	17	1172	2.6	156	0.8	64.8	-26	10.8
2	1	1.5	7838	15	1176	2.3	93	0.83	78.4	-15	7.3
2	2	0.5	6600	18	1188	4.7	316	0.55	22.2	-53.5	21.1
2	2	1.0	8024	15	1204	10.6	803	0.37	21.3	-56.8	29.5
2	2	1.5	9896	12	1188	24.8	1440	0.35	12	-60	31.4
3	0	0.0	6000	20	1200	4.2	291	0.67	18.2	-73	36.9
3	1	0.5	6195	19	1177	7.2	328	0.6	36.6	-62.4	24.1
3	1	1.0	6744	18	1214	2.7	169	0.81	62.6	-24.2	11.8
3	1	1.5	7563	16	1210	2.2	101	0.82	74.1	-13.8	7.7
3	2	0.5	6353	19	1207	5.1	406	0.55	20.6	-69.7	27.4
3	2	1.0	7309	16	1169	9.7	715	0.43	20.1	-58	30.7
3	2	1.5	8666	14	1213	18.4	1294	0.42	14.5	-54.7	44.6
4	0	0.0	6001	20	1200	4.1	288	0.67	18.6	-87.9	40.1
4	1	0.5	6482	19	1232	5.5	292	0.56	20.6	-81.5	35.7
4	1	1.0	7673	16	1228	11	252	0.48	21.2	-73	22.8
4	1	1.5	9262	13	1204	17.2	304	0.59	11	-71.7	36.1
4	2	0.5	6310	19	1199	4.2	392	0.66	28.5	-64.5	22.1
4	2	1.0	7156	17	1217	5.3	694	0.65	39.8	-54.8	21.3
4	2	1.5	8366	14	1171.24	9.4	1036	0.62	26.1	-54.1	21.1
5	0	0.0	6001	20	1200	4.2	287	0.67	18.2	-78.4	37.2
5	1	0.5	6253	19	1188	5.4	321	0.63	31.7	-69.7	26.8
5	1	1.0	6954	17	1182	7.3	294	0.71	43.6	-40.3	16.6
5	1	1.5	7975	15	1196	9.3	329	0.7	31.3	-36.3	13.9
5	2	0.5	6502	18	1170	5.9	305	0.54	19.4	-60.8	18.1
5	2	1.0	7721	16	1235	7.6	521	0.36	25.5	-42.8	15.6
5	2	1.5	9328	13	1213	24.3	1394	0.47	9.8	-63.3	35.1
6	0	0.0	6001	20	1200	4.1	294	0.66	18	-38.5	26.2
6	1	0.5	6329	19	1203	6.4	299	0.64	25	-40.1	17.6
6	1	1.0	7204	17	1225	2.5	150	0.85	48.6	-21.6	11.2
6	1	1.5	8440	14	1182	2.2	91	0.89	44.4	-12.7	7.2
6	2	0.5	6611	18	1190	7.3	590	0.41	17.1	-51	46
6	2	1.0	8120	15	1218	10.5	874	0.33	14.2	-38.2	31.1
6	2	1.5	10090	12	1211	23.5	1860	0.35	8.9	-36.3	34.4

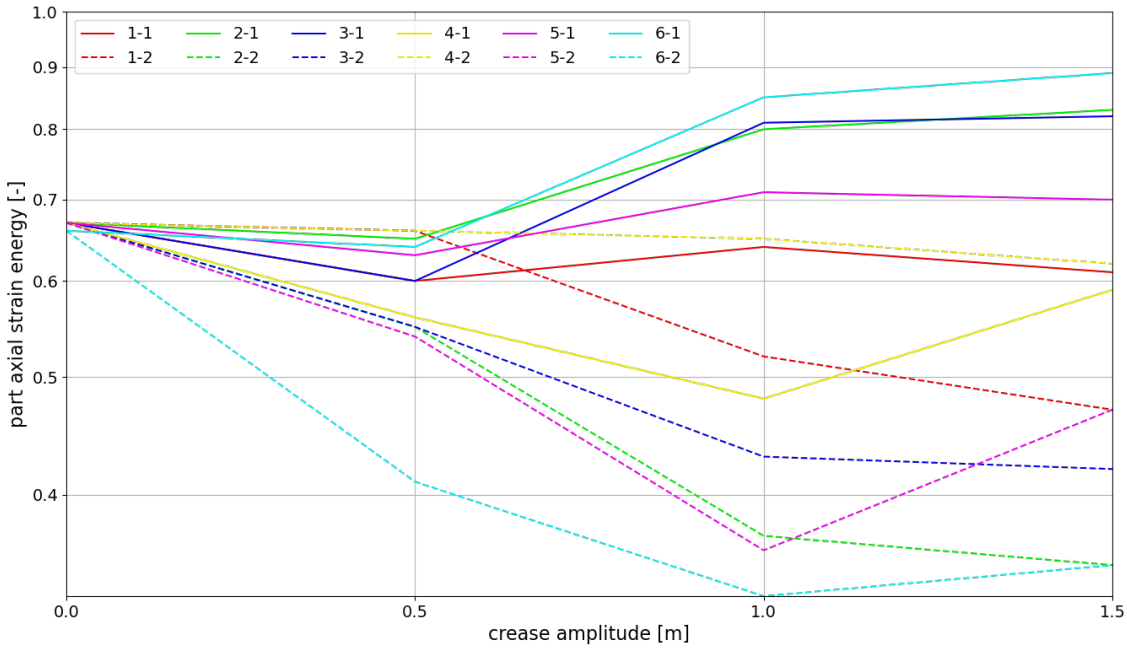

Figure 14: *Influence of the introduction of creases with different topologies, directions, and amplitudes on the contribution of the axial strain energy in the total strain energy*

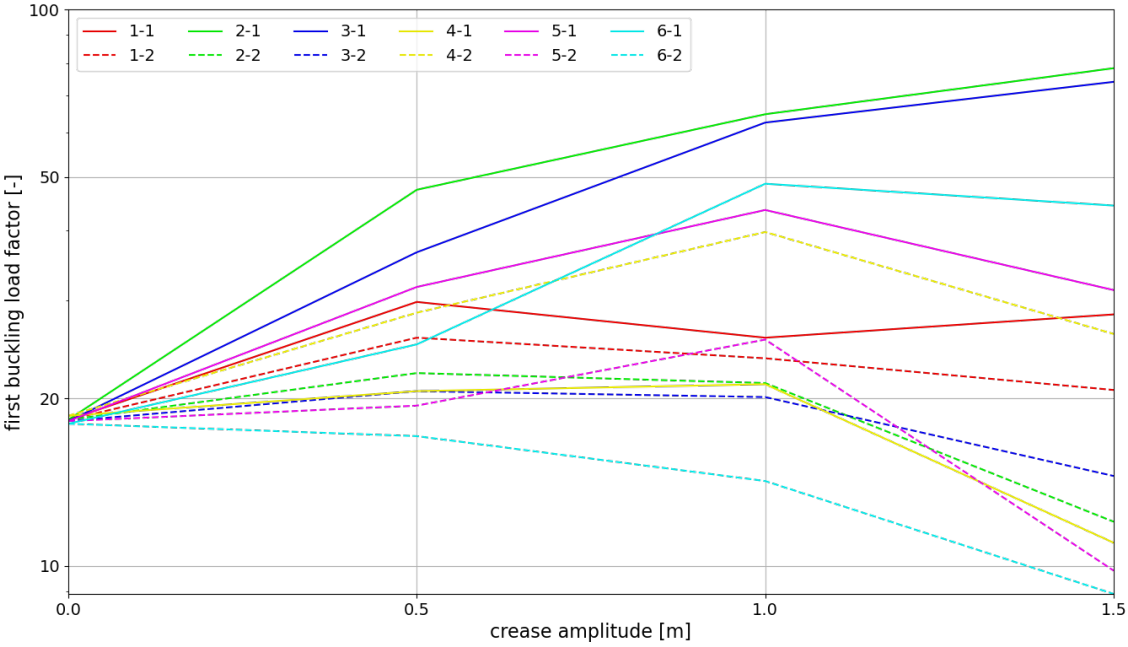

Figure 15: *Influence of the introduction of creases with different topologies, directions, and amplitudes on the first buckling load factor*